

## DYNAMICAL MASSES OF T TAURI STARS AND CALIBRATION OF PRE-MAIN-SEQUENCE EVOLUTION

M. SIMON

Department of Physics and Astronomy, State University of New York, Stony Brook, NY 11794-3800; msimon@sbast1.ess.sunysb.edu

AND

A. DUTREY AND S. GUILLOTEAU

Institut de Radio Astronomie Millimétrique, 300 Rue de la Piscine, F-38406 Saint Martin d'Hères, France

Received 2000 April 4; accepted 2000 August 18

### ABSTRACT

We have used the high sensitivity and resolution of the IRAM interferometer to produce subarcsecond  $^{12}\text{CO } J = 2-1$  images of nine protoplanetary disks surrounding T Tauri stars in the Taurus-Auriga cloud (seven singles and two binaries). The images demonstrate the disks are in Keplerian rotation around their central stars. Using the least-square fit method described in the 1998 work by Guilloteau & Dutrey, we derive the disk's properties, in particular its inclination angle and rotation velocity, hence the dynamical mass. Since the disk mass is usually small, this is a *direct* measurement of the stellar mass. Typically, we reach an internal precision of 10% in the determinations of stellar mass. The overall accuracy is limited by the uncertainty in the distance to a specific star. In a distance-independent way, we compare the derived masses with theoretical tracks of pre-main-sequence evolution. Combined with the mean distance to the Taurus region (140 pc), for stars with mass close to  $1 M_{\odot}$ , our results tend to favor the tracks with cooler photospheres (higher masses for a given spectral type). We find that in UZ Tau E, the disk and the spectroscopic binary orbit appear to have different inclinations.

*Subject headings:* binaries: close — circumstellar matter — radio lines: stars — stars: individual (BP Tauri, CY Tauri, DL Tauri, DM Tauri, GG Tauri, GM Aurigae, LkCa 15, MWC 480, UZ Tauri) — stars: pre-main-sequence — stars: variables: other

### 1. INTRODUCTION

Nearly all of our knowledge about the masses and ages of low-mass young stars comes from their location in the H-R diagram relative to theoretical calculations of stellar evolution to the main sequence. Despite considerable advances over the past 5–10 years in understanding the structure and atmospheres of stars of mass  $M < 1 M_{\odot}$ , comparison of the currently available predicted evolutionary paths of young stars shows obvious differences. Empirical tests of the calculations have not been possible until recently because astronomers have not had independent measurements of either the mass or age of a young star. This situation is changing rapidly. One way to test the calculated tracks is to investigate whether they yield the same ages for stars expected to be coeval on physical grounds. Hartigan, Strom, & Strom (1994), Casey et al. (1998), and White et al. (1999) have applied this test to wide binaries, the TY CrA system, and the GG Tau system, respectively, using tracks available at the time. Over a mass range extending down to the brown dwarfs, they found significant differences in the extent to which the several theoretical calculations satisfy the coevality requirement.

The capability of millimeter-wave interferometers to resolve the spectral line emission of the outer disks of pre-main-sequence (PMS) stars offers the possibility to map their rotation. Since the disk mass is usually very small compared to the mass of the star, this provides the means to measure the stellar mass dynamically (e.g., Dutrey, Guilloteau, & Simon 1994, hereafter DGS94; Guilloteau & Dutrey 1998, hereafter GD98). We use this technique to obtain new measurements of the mass of five single PMS stars and one PMS binary. Combined with our previous measurements of the PMS single GM Aur and the binary

GG Tau (Dutrey et al. 1998; Guilloteau, Dutrey, & Simon 1999), the measured stellar masses span the range  $\sim 2$  to  $0.5 M_{\odot}$ . We use the results to test the theoretical calculations of PMS evolution. Section 2 describes the sample of stars and the interferometric observations. Section 3 summarizes the analysis and presents the measured masses and related parameters. Section 4 compares the measured masses with those implied by location of the stars in the H-R diagram relative to the tracks calculated by d'Antona & Mazzitelli (1997, hereafter DM97),<sup>1</sup> Baraffe et al. (1998, hereafter BCAF), Palla & Stahler (1999, hereafter PS99), and Siess, Dufour, & Forestini (2000, hereafter SDF).<sup>2</sup>

### 2. SAMPLE OF STARS AND INTERFEROMETER OBSERVATIONS

#### 2.1. Sample of Stars

All the stars studied are in Taurus-Auriga (Table 1). We obtained new interferometric observations in the  $^{12}\text{CO } J = 2-1$  line of the singles CY Tau, DL Tau, DM Tau, LkCa 15, and MWC 480 (HD 31648), and the spectroscopic binary UZ Tau E (Mathieu, Martin, & Maguzzu 1996). They were selected because earlier interferometric observations (Table 1, col. [5]) indicated that they were, or were likely to be, associated with resolvable circumstellar disks. BP Tau was observed because its *Hipparcos* distance,  $56 \pm 14$  pc (Favata et al. 1998), is very different from the 140 pc average distance to the Taurus star-forming region (Kenyon, Dobrzycka, & Hartmann 1994), suggesting that it is much older than previously thought (see also Bertout,

<sup>1</sup> See also <http://venus.mporzio.astro.it/~dantona/>.

<sup>2</sup> See also <http://www-laog.obs.ujf-grenoble.fr/activites/starevol/evol.html>.

TABLE 1  
PARAMETERS OF PROGRAM STARS

Name (1)	Spectral Type (2)	$L_*/L_\odot$ (3)	$T_{\text{eff}}$ (K) (4)	References <sup>a</sup> (CO) (5)	References <sup>b</sup> ( $L_*$ , $T_{\text{eff}}$ ) (6)
Singles					
MWC 480.....	A4	11.5	8460	1	1
LkCa 15.....	K5	0.74	4350	2	...
DL Tau.....	K7	0.68	4060	3	2
GM Aur.....	K7	0.74	4060	4	3
BP Tau.....	K7	0.93	4060	...	4
DM Tau.....	M1	0.25	3720	5	...
CY Tau.....	M1	0.47	3720	3	...
Binaries					
GG Tau Aa.....	K7	0.84	4060	6	5
GG Tau Ab.....	M0.5	0.71	3800	...	...
UZ Tau E.....	M1	1.60	3720	3, 7	...

<sup>a</sup> References to col. (5): (1) Mannings & Sargent 1997; (2) Duvert et al. 2000; (3) Dutrey et al. 1996; (4) Dutrey et al. 1998; (5) Guilloteau & Dutrey 1998; (6) Guilloteau, Dutrey, & Simon 1999; (7) Jensen, Koerner, & Mathieu 1996.

<sup>b</sup> References to col. (6): (1)  $L_*$  from Malfait et al. 1998 and this work, and spectral type from C. Grady, 1999, private communication; (2)  $L_*$  from Hartigan, Edwards, & Ghandour 1995; (3) spectral type and  $L_*$  from Gullbring et al. 1998; (4) see Favata et al. 1998 and § 4.1; (5)  $L_*$  and spectral type from White et al. 1999.

Arenon, & Robichon 1999). Mass measurements of the single GM Aur and the binary GG Tau Aa by  $^{12}\text{CO } J = 2-1$  line interferometric mapping have already been reported (Dutrey et al. 1998 and Guilloteau et al. 1999). We included DM Tau in our program because new data at three times better angular resolution would provide an independent check on the method and earlier results (GD98).

Table 1 provides spectral types, luminosities, and effective temperatures for our sample. Most of the spectral types and stellar luminosities,  $L_*$ , in columns (2) and (3) of Table 1 are taken from Kenyon & Hartmann (1995). The luminosities are the  $L_J$  in their Table A4. All the luminosities in column (3) are evaluated at 140 pc distance. The actual distances to the individual stars are important for our analysis but are presently unknown; we will discuss this problem in § 4. The effective temperatures in column (4),  $T_{\text{eff}}$ , corresponding to the spectral types, for all the stars, are obtained using Table A1 of Kenyon & Hartmann (1995) for main-sequence stars; we discuss the spectral type to  $T_{\text{eff}}$  conversion further in § 4.

## 2.2. Interferometer Observations

Our IRAM interferometer observations used five antennas operating in snapshot mode (Guilloteau et al. 1992; Dutrey et al. 1996) and were carried out in the winter of 1997/1998. For BP Tau, the full synthesis mapping was obtained in the winter of 1998/1999. We observed all the sources simultaneously at 89.2 ( $\text{HCO}^+ J = 1-0$ ) GHz and 230.5 GHz ( $^{12}\text{CO } J = 2-1$ ). The spectra were analyzed using a correlator with one band of 10 MHz centered on the  $\text{HCO}^+ J = 1-0$  line, one band of 20 MHz centered on the  $^{12}\text{CO } J = 2-1$  line, two bands of 160 MHz for the 1.3 mm and 3.4 mm continuum, respectively. The spectral resolution was 0.23 and 0.18  $\text{km s}^{-1}$  in the narrow bands at 3.4 and 1.3 mm, respectively. The phase calibrators were 0415 + 379 (3C 111) and PKS 0528 + 134. The rms phase noise was  $8^\circ$  to  $25^\circ$  and  $15^\circ$  to  $50^\circ$  at 3.4 and 1.3 mm,

respectively, which introduced position errors of less than  $0''.1$ . The seeing, estimated from observations of the calibrators, was  $\sim 0''.3$ . Baselines up to 400 m provided  $\sim 0''.7$  resolution for the 1.3 mm continuum data and  $1''.8$  at 3.4 mm. The flux scale was checked by observation of MWC 349, which has been used as a calibrator at IRAM since 1996. Its flux is given by  $S_\nu = 0.93 \times (\nu/87)^{0.6}$  Jy, following Altenhoff et al. (1981), and subsequent measurements of the planets made at IRAM (IRAM Flux Report 13).

The GILDAS software package was used to reduce the data. At 1.3 mm, the continuum images are the results of summing the lower and the upper sideband data. At 3.4 mm, the tuning was purely in the lower sideband. The continuum and line maps were produced using natural weighting of the visibilities. For clarity, tapering to about  $1''$  resolution was used on line maps presented in Figures 1 and 2, but the full angular resolution was used in the fitting of models by the  $\chi^2$  technique. We did not subtract the continuum emission from the CO map because its contribution is small, but we included it in the analysis.

## 3. ANALYSIS AND RESULTS

The essential inputs are the angularly resolved maps of the CO line emission at each velocity channel and the “standard” model of a rotating disk in hydrostatic equilibrium (e.g., DGS94). We use the procedure developed by GD98 to derive the parameters of the model by the method of  $\chi^2$  minimization. To avoid nonlinear effects arising from deconvolution, the  $\chi^2$  minimization is performed in the  $(u, v)$ -plane. The derived parameters divide naturally into those relevant for the determination of the central mass and those that pertain mostly to the properties of the disk. Here, with the exception of DM Tau, for which we summarize the complete analysis, we will concentrate on the parameters required to determine the central mass—the disk inclination  $i$  and position angle P.A.,  $V \sin i$  at  $r = 100$  AU, the exponent  $\nu$  of the rotation curve  $V(r/r)^{-\nu}$  and the outer

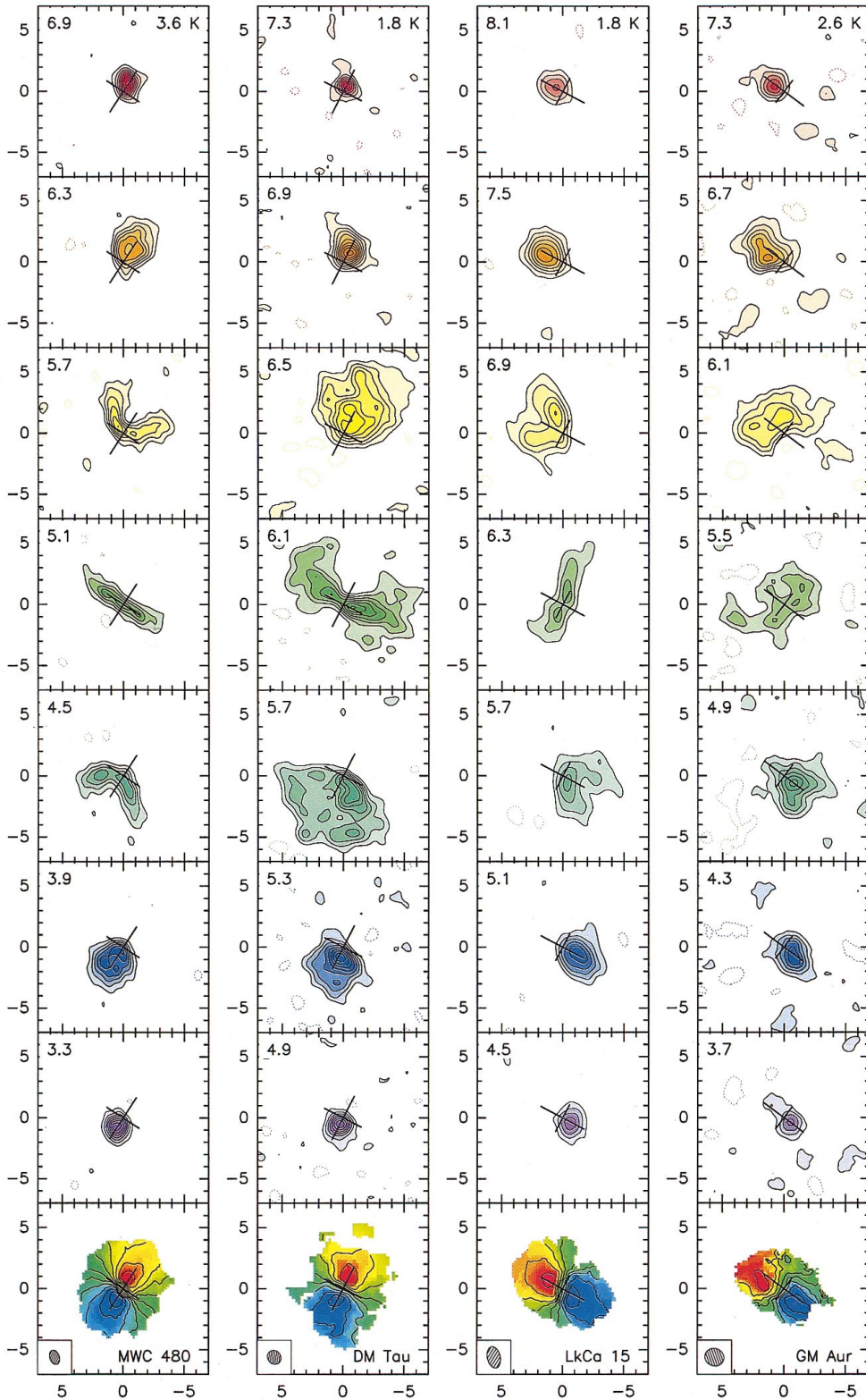


FIG. 1a

FIG. 1.—(a) Results of our interferometric observations of MWC 480, DM Tau, LkCa 15, and GM Aur. The coordinates are arcseconds in right ascension and declination centered on the peaks of the continuum emission (Table 2). The long and short arms of the crosses, centered on these positions, indicate the apparent major and minor axes of the disks. The long arms point in the direction of  $PA_{CO}$  (Table 4). The top seven panels for each object are velocity channel maps with the velocity ( $\text{km s}^{-1}$ ) with respect to the local standard of rest indicated in the upper left-hand corner. The contour spacing, different for each object, is indicated in upper right-hand corner of the top panel. The contour spacing is  $2.7 \sigma$  on average but varies from source to source; the smallest value is  $2.2 \sigma$  for DL Tau in Fig. 2. The bottom panel shows the velocity gradient map for each object, color-coded so that red indicates redshift with respect to the systemic velocity. The velocity contour spacing ( $\text{km s}^{-1}$ ) in these panels is: MWC 480, 0.3; DM Tau, 0.2; LkCa 15, 0.3; GM Aur, 0.3. (b) Same as (a) but for UZ Tau E, CY Tau, DL Tau, and BP Tau. The nearly emission-free channels at  $V_{\text{lsr}} = 6.6 \text{ km s}^{-1}$  (UZ Tau) and  $V_{\text{lsr}} = 5-6.6 \text{ km s}^{-1}$  (DL Tau) are the result of confusion with the molecular cloud. The velocity contour spacing for the velocity gradient maps in the bottom panels are, in  $\text{km s}^{-1}$ : UZ Tau, 0.6; CY Tau, 0.2; DL Tau, 0.4; BP Tau, 0.3.

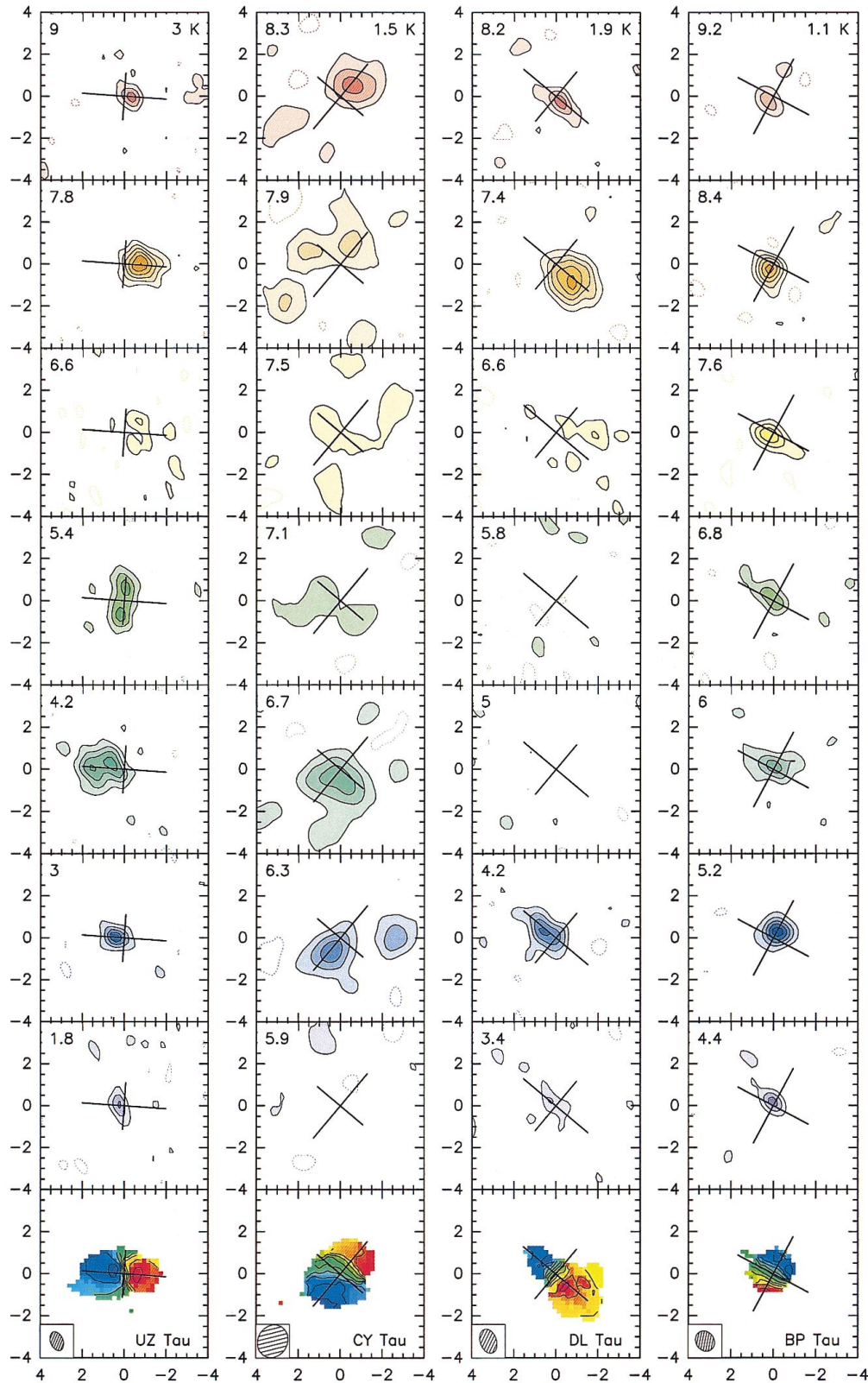


FIG. 1b

disk radius  $R_{\text{out}}$ . A paper describing the disk parameters (e.g., the temperature radial distribution, the  $^{12}\text{CO}$  abundance and spectral line turbulence width) is in preparation.

GD98 demonstrated the  $\chi^2$  parameter-fitting procedure by applying it to  $^{12}\text{CO}$   $J = 1-0$  data for the single star DM Tau. They used  $D = 150$  pc for the distance to DM Tau.

Since we now adopt 140 pc as the reference distance, we scale GD98's results to this value. On this basis, GD98's value for DM Tau's mass is  $(0.47 \pm 0.06) \times (D/140 \text{ pc}) M_{\odot}$  (see Table 3). Figure 1 shows seven of the velocity channel maps measured in the  $^{12}\text{CO}$   $J = 2-1$  line for all the sources in our sample. Figure 1 also presents velocity gradient maps

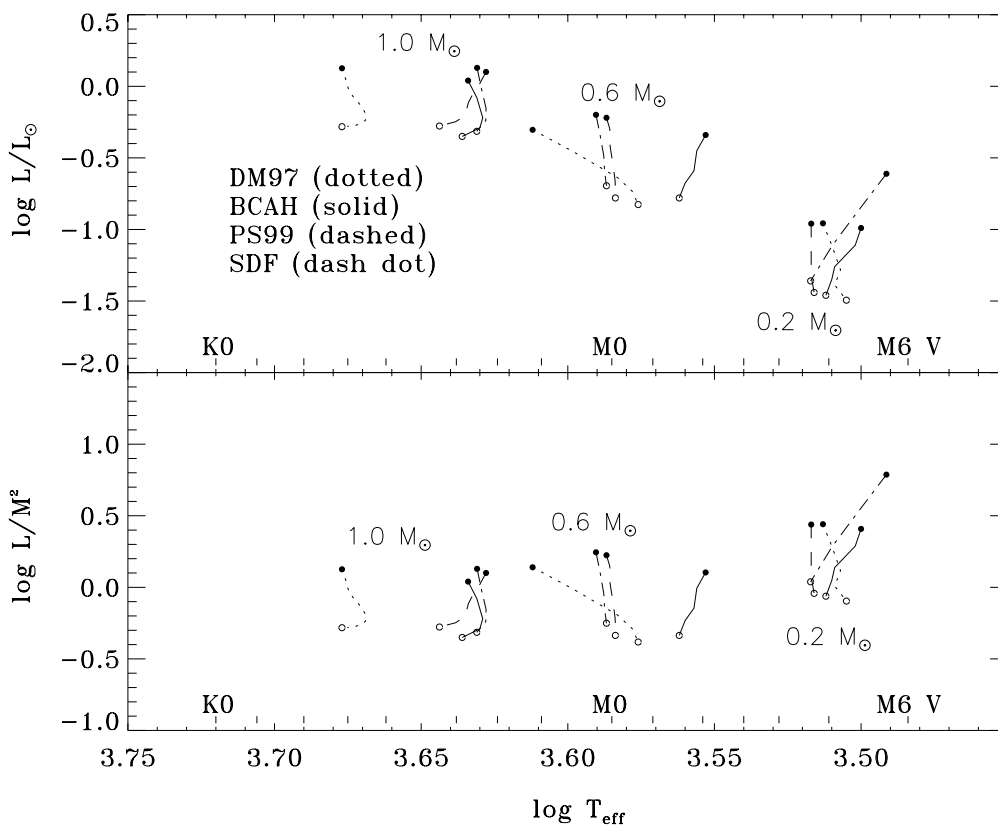


FIG. 2.—(Top) An H-R diagram showing theoretical evolutionary tracks for stars of mass 0.2, 0.6, and  $1.0 M_{\odot}$  calculated by DM97, BCAH, PS99, and SDF between the ages 2 MY (filled circles) and 10 MY (open circles). (Bottom) Same tracks as in upper panel plotted as  $L/M^2$  vs.  $T_{\text{eff}}$  (see text). The spectral type/effective temperature conversion is that of Kenyon & Hartmann 1995—see text.

that show on the redshifted and blueshifted sides of the systemic velocity, the characteristic CO emission pattern attributable to rotation of a tilted disk.

Figure 1a shows that DM Tau, GM Aur, LkCa 15 and MWC 480 appear to have no CO emission from the parent cloud. UZ Tau E and DL Tau (Fig. 1b) suffer some confusion with the CO emission of the cloud. Confusion is maximum at the cloud systemic velocity, which is usually (but not always, see DL Tau) the stellar velocity. Hence, it preferentially affects the disk emission, which is elongated along the projected disk minor axis. This results in an incorrect estimate of the disk inclination. In the case of CY Tau, we cannot be sure about the level of confusion because of the weakness of its CO emission. For UZ Tau E and DL Tau, the velocity channels hidden by the foreground CO cloud have been removed from the  $\chi^2$  analysis. In the case of UZ Tau E, four of 36 significant channels were removed. In the case of DL Tau, five of 18 significant channels had to be removed because of confusion. This increased the uncertainty in the disk inclination quite significantly.

The first step of the model fitting procedure is to measure the coordinates of the millimeter-wave continuum source in order to recenter the  $(u, v)$ -plane visibilities on it. Table 2 lists these source coordinates for DM Tau and for the other stars newly observed for this program. The UZ Tau E spectroscopic binary cannot be resolved by our observations; its continuum source coordinates must be effectively centered on the binary.

Table 3 compares the results of the full analysis of DM Tau obtained by GD98 from their analysis of the  $^{12}\text{CO}$

$J = 1-0$  data at  $\sim 3''$  resolution with that derived from our new  $^{12}\text{CO } J = 2-1$  data. Only the fitted parameters are shown; the gas density and  $^{12}\text{CO}$  abundance are the same in the two analyses and do not affect the stellar mass determination because the  $^{12}\text{CO } J = 1-0$  and  $J = 2-1$  lines are optically thick. We scaled GD98's values of the parameters that depend on physical size, and hence distance, from the 150 pc distance to the 140 pc distance used here. The uncertainties are the formal  $2\sigma$  values from the  $\chi^2$  fit. The position angles in Table 3 refer to the major axis of the disk; the P.A. listed in GD98 is that for the disk rotation axis so differs by  $90^\circ$  from the P.A.<sub>CO</sub> given here. The agreement between GD98 and the new results is excellent for all the

TABLE 2  
MEASURED MILLIMETER CONTINUUM SOURCE  
COORDINATES (J2000.0)

Name	Right Ascension	Declination
MWC 480.....	04 58 46.264	29 50 37.03
LkCa 15.....	04 39 17.784	22 21 03.46
DL Tau .....	04 33 39.074	25 20 38.14
DM Tau .....	04 33 48.731	18 10 10.00
CY Tau .....	04 17 33.727	28 20 46.95
UZ Tau E.....	04 32 43.070	25 52 31.14
BP Tau.....	04 19 15.835	29 06 26.90

NOTE.—Units of right ascension are hours, minutes, and seconds, and units of declination are degrees, arcminutes, and arcseconds. The astrometric accuracy is better than  $0''.05$ .

TABLE 3  
COMPARISON OF OLD AND NEW RESULTS FOR DM TAU

Parameter	GD98	This Work
Systemic velocity— $V_{\text{LSR}}$ (km s $^{-1}$ ) .....	$6.05 \pm 0.02$	$6.01 \pm 0.01$
Orientation—P.A. $_{\text{CO}}$ (deg) .....	$-25 \pm 2$	$-23 \pm 1$
Inclination— $i$ (deg) .....	$33 \pm 2$	$-32 \pm 2$
Outer radius— $R_{\text{out}}$ (AU).....	$793 \pm 20$	$800 \pm 5$
Turbulent line width— $\Delta v$ (km s $^{-1}$ ) .....	$0.08 \pm 0.03$	$0.07 \pm 0.02$
Temperature law: $T(r) = T_{100}(\frac{r}{100\text{AU}})^{-q}$		
Temperature at 100 AU— $T_{100}$ (K) .....	$31 \pm 2$	$32.5 \pm 0.5$
Temperature exponent— $q$ .....	$0.63 \pm 0.05$	$0.63 \pm 0.01$
Velocity law: $V(r) = V_{100}(\frac{r}{100\text{AU}})^{-v}$		
$V \sin i$ at 100 AU— $V_{100} \sin i$ (km s $^{-1}$ ).....	$1.11 \pm 0.03$	$-1.17 \pm 0.02$
Velocity exponent— $v$ .....	$0.57 \pm 0.04$	$0.53 \pm 0.01$
Stellar mass— $M_*$ ( $M_{\odot}$ ).....	$0.47 \pm 0.06$	$0.55 \pm 0.07$

NOTE.—Comparison of parameters derived from CO(1–0) (GD98) and CO(2–1) (this work) in DM Tau.

parameters except for the inclination, which now has the opposite sign. It is not surprising that the higher resolution data better define the sense of the inclination. Its sign does not affect the mass determination.

Table 4 lists the parameters most relevant for determination of the central mass derived from our new observations and also from our previously published observations. Columns (2) and (3) are described below. Columns (4) and (5) list the disk P.A. and  $i$  derived from the CO line maps. The disk outer radius,  $R_{\text{out}}$ , in column (6) is included here because its determination and that of  $i$  are coupled (see, for example, GD98 § 4.4). Column (6) lists the value of  $V \sin i$  at the reference radius 100 AU and column (7) lists the exponent of the radial power-law dependence of the velocity. Within the uncertainties, the rotation is Keplerian. The stellar masses in column (8) are derived using

$$M = \left\{ \frac{(V_{100} \sin i)}{2.98 \sin i} \right\}^2 M_{\odot}, \quad (1)$$

where  $2.98 \text{ km s}^{-1}$  is the circular velocity at 100 AU radius from a  $1 M_{\odot}$  star. The derived masses scale as  $M_* \propto v^2(r)r$  and, hence, depend on distance to the star as  $M_* \propto D$ . The

main source of uncertainty in the measured stellar mass is the inclination; the two objects in our sample with the lowest inclinations, CY Tau and BP Tau, have the highest uncertainties in their derived masses. This approach ignores the mass of the disk because it is usually only a few percent of that of the star. Even in GG Tau A, which probably has the most massive disk of the stars in our sample, the mass of the circumbinary is only  $\sim 10\%$  that of the stars within it (Guilloteau et al. 1999). It is interesting that UZ Tau E has a circumbinary ring like GG Tau A and UY Aur (Duvert et al. 1998), although the central hole is as yet unresolved.

The 1.3 mm continuum emission is detected by a separate backend (§ 2.2) and the detected continuum emission arises mostly from the innermost regions of the disk (see below). The continuum images can therefore provide independent measurements of the disk orientation. Columns (2) and (3) of Table 4 give the position angle, P.A. $_{\text{cont}}$ , of the major axis of the disk, and its inclination,  $i_{\text{cont}}$ , measured from the 1.3 mm wavelength continuum image. To derive the inclination from the ratio of apparent major and minor axes, we used an effective seeing of  $0''.3$ . We did not include uncertainty in the seeing in the error estimate. The agreement between the orientations and inclinations derived from 1.3 mm contin-

TABLE 4  
DERIVED PARAMETERS ( $D = 140 \text{ pc}$ )

Star (1)	PA $_{\text{cont}}$ (deg) (2)	$i_{\text{cont}}$ (deg) (3)	PA $_{\text{CO}}$ (deg) (4)	$i_{\text{CO}}$ (deg) (5)	$R_{\text{out}}$ (AU) (6)	$V_{100} \sin i$ (km s $^{-1}$ ) (7)	$-v$ (8)	$M_*$ ( $M_{\odot}$ ) (9)
Singles								
MWC 480 .....	$-10 \pm 11$	$26 \pm 7$	$-32 \pm 1$	$+38 \pm 1$	$545 \pm 5$	$-2.38 \pm 0.02$	$0.50 \pm 0.02$	$1.65 \pm 0.07$
LkCa 15 .....	$62 \pm 5$	$42 \pm 5$	$+61 \pm 1$	$+52 \pm 1$	$650 \pm 15$	$-2.30 \pm 0.02$	$0.56 \pm 0.03$	$0.97 \pm 0.03$
DL Tau <sup>a</sup> .....	$44 \pm 3$	$49 \pm 3$	$+50 \pm 3$	$+35 \pm 2$	$520 \pm 50$	$1.90 \pm 0.06$	$0.55 \pm 0.03$	$0.72 \pm 0.11$
GM Aur .....	$57 \pm 5$	$54 \pm 5$	$+51 \pm 2$	$+56 \pm 2$	$525 \pm 20$	$2.30 \pm 0.08$	$0.5 \pm 0.1$	$0.84 \pm 0.05$
DM Tau .....	$-1 \pm 5$	$45 \pm 5$	$-27 \pm 1$	$-32 \pm 1$	$800 \pm 5$	$-1.17 \pm 0.02$	$0.53 \pm 0.01$	$0.55 \pm 0.03$
CY Tau .....	$-56 \pm 7$	$47 \pm 8$	$-30 \pm 7$	$+30 \pm 10$	$270 \pm 10$	$-1.10 \pm 0.10$	$0.50 \pm 0.08$	$0.55 \pm 0.33$
BP Tau .....	...	$20 \pm 20$	$-28 \pm 3$	$+30^{+4}_{-2}$	$108 \pm 4$	$1.67 \pm 0.06$	$0.54 \pm 0.07$	$1.24^{+0.25}_{-0.32}$
Binaries								
GG Tau A.....	$7 \pm 2$	$37 \pm 1$	$+7 \pm 2$	$+37 \pm 1$	$\sim 800$	$2.05 \pm 0.06$	$0.5 \pm 0.1$	$1.28 \pm 0.07$
UZ Tau E .....	$87 \pm 3$	$54 \pm 3$	$+86 \pm 2$	$-56 \pm 2$	$300 \pm 20$	$-2.83 \pm 0.05$	$0.53 \pm 0.03$	$1.31 \pm 0.08$

<sup>a</sup> No sign for  $i_{\text{cont}}$ ; using the inclination derived from the continuum (see text).

uum data and  $^{12}\text{CO } J = 2-1$  data is excellent for most of the targets. The uncertainties of the values derived from the continuum images are larger, in most cases, than those from the CO data because the measured sizes of the disks in the continuum are generally smaller than in CO, especially when the inclinations are low. The sizes measured in the continuum are smaller because the dust continuum opacity is much smaller than in the CO line. The detected continuum emission therefore arises mostly in the dense inner regions of the disks (see, for example, Dutrey et al. 1996). The values for CY Tau suffer from a low signal-to-noise ratio. In the case of DL Tau, significant confusion from the molecular cloud seems to have affected the determination of the inclination from the CO emission (§ 3). The confusion affects the channels near the systemic velocity, which are the most important to determine the inclination. Accordingly, pending better measurements (e.g.,  $^{13}\text{CO}$ ), we prefer to use the inclination determined from the continuum emission,  $\sim 45^\circ$ , to derive the mass for DL Tau. With this inclination, the stellar mass is  $0.72 \pm 0.11 M_\odot$  rather than  $1.23 \pm 0.11 M_\odot$  when using the CO-derived inclination.

#### 4. COMPARISON OF THE MEASURED MASSES AND THEORETICAL TRACKS

##### 4.1. The Theoretical Tracks

The observational measure of the stellar photospheric temperature is its spectral type while the parameter provided by the models is usually  $T_{\text{eff}}$ . The surface gravities of the PMS stars lie between those of the main-sequence stars and giants so the conversion between spectral type and  $T_{\text{eff}}$  determined for the giants and dwarfs may not apply. White et al. (1999) and Luhman (1999), in addition to others, have investigated this problem and demonstrate that the differences in temperature scales become apparent for the lowest mass stars and below the hydrogen-burning limit. Luhman (1999) proposed an “intermediate” temperature scale for the M stars. Its differences from Kenyon & Hartmann’s (1995) temperature scale become significant for stars cooler than about M6. Since our sample does not include stars as cool as this, we use the Kenyon and Hartmann scale in the present work without modification.

The H-R diagram in Figure 2 (*top panel*) shows excerpts from PMS tracks calculated by DM97, BCAH, PS99, and SDF. In this and subsequent figures, the BCAH tracks for  $M/M_\odot < 0.7$  are for mixing length parameter (mixing length/pressure scale height) = 1.0 and 1.9 for  $M/M_\odot \geq 0.7$  (BCAH and I. Baraffe, 1998, private communication). Differences among the theoretical calculations for a star of given age and mass are obvious. For example, the DM97 tracks are hotter than those of BCAH for  $M_* \sim 0.2 M_\odot$ . SDF’s models at 0.2 and 0.1  $M_\odot$  appear to contract more slowly than those of DM97, BCAH, and PS99. Since the different treatments of stellar convection, the equation of state, opacities, and stellar atmospheres become important in specific regions of the H-R diagram, tests of the theoretical tracks require accurate measurements of mass over as wide a range of mass and age as possible.

The dependence of  $M_*$  on distance (§ 3) is important because while the average distance to the Taurus star-forming region (SFR) is reasonably well known, the actual distance to a given star in it is not. The Taurus SFR extends for at least  $15^\circ$  on the sky. If its depth is comparable to its width, the distance to a specific member may scatter by

$\pm 20$  pc around the 140 pc mean, a relative error of  $\pm 14\%$ . Only CY Tau and BP Tau (Table 4) have a larger uncertainty of their mass measurement. For most of the stars in Table 4, the uncertainty in their actual mass is therefore dominated by the uncertainty in their distance. The distance, of course, also determines the star’s location in the H-R diagram because  $L_* \propto D^2$ . Therefore, we will present most of our results in § 4 on modified H-R diagrams in which the distance-independent parameter  $L/M^2$  is plotted versus  $T_{\text{eff}}$ . For reference, Figure 2 (*bottom panel*) compares the tracks on this basis.

##### 4.2. Measured Masses on Theoretical H-R Diagrams: The Single Stars

Figure 3 plots the single T Tauri stars in our sample on modified H-R diagrams using PMS tracks calculated by DM97, BCAH, PS99, and SDF. The uncertainties displayed along the horizontal axis are  $\pm 1$  spectral type subclass. Along the vertical axis, the uncertainties are the propagated internal uncertainties in stellar mass (Table 4) and an assumed  $\pm 10\%$  uncertainty in the luminosity given in Table 1. We discuss the fit of each star to the theoretical tracks separately.

*LkCa 15.*—The  $L/M^2$  value for LkCa 15 lies near the 1.0  $M_\odot$  tracks calculated by BCAH, PS99, and SDF (Fig. 3) consistent with its mass  $0.97 \pm 0.03 M_\odot$  at the nominal 140 pc distance (Table 4). These tracks yield a consistent age estimate of 3–5 Myr. LkCa 15’s  $L/M^2$  values lay on the 0.8  $M_\odot$  track calculated by DM97. Agreement with the DM97 track would require a distance of  $\sim 115$  pc but would not affect the age estimate.

*DL Tau.*—The position of DL Tau’s  $L/M^2$  in the diagrams is within one spectral type uncertainty of the 0.8  $M_\odot$  track for each of the calculations. This is in good agreement with the mass derived using the continuum inclination,  $0.72 \pm 0.11 M_\odot$ . The theoretical tracks yield a consistent age estimate of  $\sim 2$  Myr.

*GM Aur.*—The position of the  $L/M^2$  value relative to the BCAH, PS99, and SDF tracks is consistent with its mass  $0.84 \pm 0.05 M_\odot$  at 140 pc. The tracks provide an age estimate of  $\sim 3$  Myr. The  $L/M^2$  value lies close to DM97’s 0.6  $M_\odot$  track, which would require a distance of 103 pc to force agreement with the dynamical mass.

*BP Tau.*—BP Tau’s  $L/M^2$  values lay between DM97’s 0.6 and 0.8  $M_\odot$  tracks and close to BCAH, PS99, and SDF’s 0.8  $M_\odot$  tracks, while our measured mass at 140 pc is in the range 0.92 to 1.49  $M_\odot$ . This suggests that the distance to BP Tau may be closer than 140 pc but not as extreme as the *Hipparcos* value,  $53_{-11}^{+17}$  pc (Favata et al. 1998). The large uncertainty in the mass produces a large spread in the age estimate, 2–10 Myr.

*DM Tau.*—Its dynamical mass at 140 pc,  $0.55 \pm 0.03 M_\odot$ , is consistent with its  $L/M^2$  value relative to four sets of tracks. The tracks yield a consistent age estimate  $\sim 5$  Myr.

*CY Tau.*—The nominal value 0.55  $M_\odot$  is consistent with its  $L/M^2$  relative to the four sets of tracks with an age in the range 2–5 Myr. However, the uncertainty in its mass is so large that this agreement is not significant, and we cannot plot it meaningfully in Figure 3.

*MWC 480 (= HD 31648).*—Figure 4 provides similar comparisons of the dynamical mass of the HAeBe star MWC 480. We calculated its stellar luminosity (Table 1) for a distance of 140 pc using the spectral energy distribution, corrected for extinction and circumstellar emission, derived

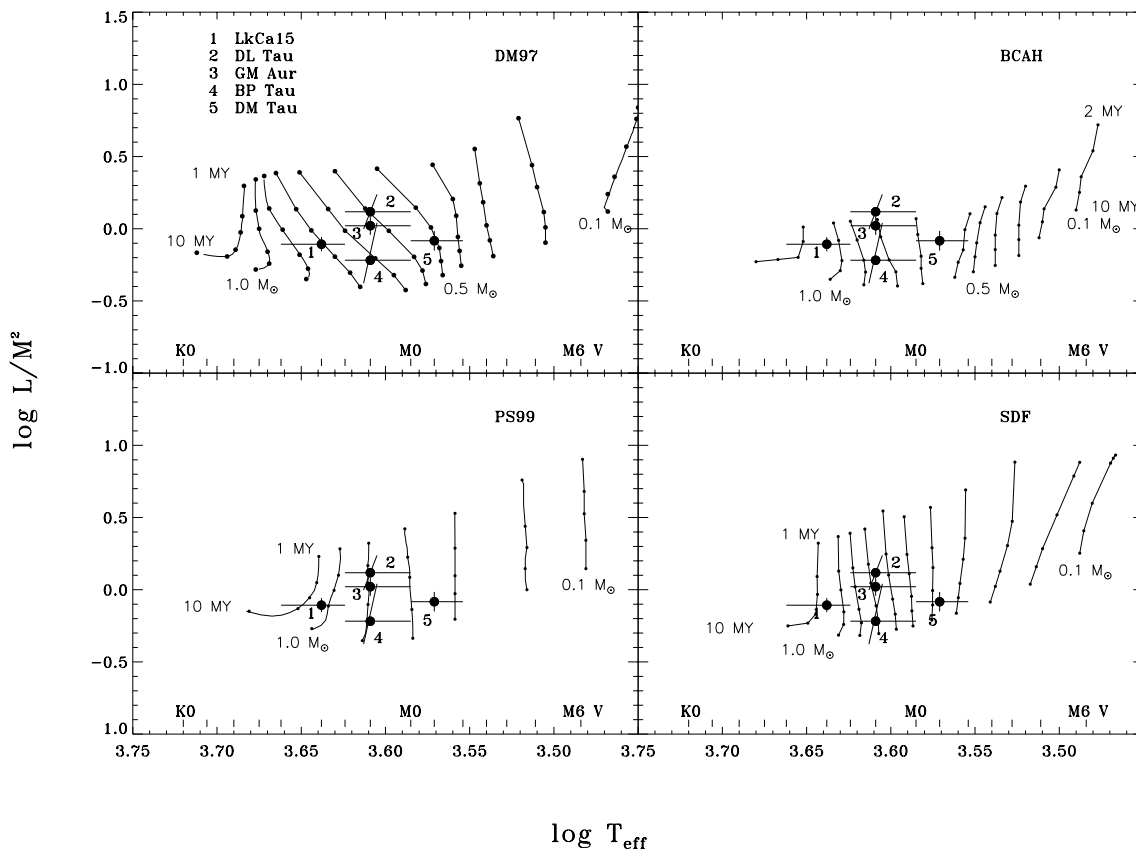


FIG. 3.—(Upper left-hand panel) Results for the single T Tauri stars plotted as  $L/M^2$  vs.  $T_{\text{eff}}$  for theoretical evolutionary tracks for stars of mass 0.1, 0.2, 0.3, 0.4, 0.5, 0.6, 0.7, 0.8, 0.9, 1.0, and  $1.2 M_{\odot}$  calculated by DM97. Filled dots are at ages 1, 2, 3, 5, 7, and 10 MY. (Upper right-hand panel) Same, but for tracks calculated by BCAH. Here the indicated ages are 2, 3, 5, 7, and 10 MY. (Lower left-hand panel) Same for tracks calculated by PS99 at masses 0.1, 0.2, 0.4, 0.6, 0.8, 1.0, and  $1.2 M_{\odot}$ . The indicated ages are 1, 2, 3, 5, and 10 MY. (Lower right-hand panel) Same for tracks calculated by SDF. The range of masses and indicated ages are same as for DM97.

by Malfait et al. (1998). This value,  $11.5 L_{\odot}$ , is about half that calculated by Mannings & Sargent (1997) from photometry available at the time. Table 1 also lists C. Grady's (1999, private communication) spectral type estimate, A4, from *HST* spectra, which is cooler than the earlier value, A2–A3, of Thé, de Winter, & Pérez (1994). BCAH PMS models do not extend to  $M > 1.2 M_{\odot}$ , so we make the comparisons only with DM97, PS99, and SDF's tracks. MWC 480's  $L/M^2$  value lies close to the  $2.0 M_{\odot}$  tracks for the three calculations at an age  $\sim 7$  Myr. The mass at 140 pc distance  $1.65 \pm 0.07 M_{\odot}$  suggests that MWC 480 lies at a somewhat greater distance. A distance of 170 pc would yield a dynamical mass of  $2.0 M_{\odot}$  and would be within  $2 \sigma$  of the *Hipparcos* measurement of  $131_{-18}^{+24}$  pc (van den Ancker, de Winter, & Tjin A Dje 1998).

#### 4.3. The Binaries

The results for the binaries cannot be plotted on  $L/M^2$  versus  $T_{\text{eff}}$  diagrams because the component luminosities of UZ Tau E or component masses of GG Tau are not known. We discuss the binaries using conventional H-R diagrams.

*UZ Tau E*.—Mathieu et al. (1996) discovered that UZ Tau E is a single-lined spectroscopic binary with period 19.1 days and projected semimajor axis of the primary  $a_1 \sin i_* = 0.03$  AU, in which  $i_*$  is the inclination of the orbit.

Our measurement of the total binary mass ( $M_1 + M_2$ ) (Table 4) and the period determine  $(a_1 + a_2) = (0.153$

$\pm 0.003)(D[\text{pc}/140])^{1/3}$  AU. We can solve for  $a_1$  and  $a_2$ , and hence  $M_1$  and  $M_2$ , if we assume that the circumbinary disk and binary orbit are coplanar,  $i_{\text{CO}} = i_*$ . This assumption yields  $M_1 = (1.00 \pm 0.08)(D[\text{pc}/140]) M_{\odot}$  and  $M_2 = (0.31 \pm 0.02)(D[\text{pc}/140]) M_{\odot}$ . We plot the primary in the H-R diagram (Fig. 5) assuming that the system spectral type M1 (Table 1) applies to the primary, assigning, as before, an uncertainty of  $\pm 1$  one subclass, and luminosity in the range 0.5 to 1 times the total system luminosity,  $1.6 L_{\odot}$ . Figure 5 shows that, with these assumptions, the primary lies in the  $\sim 0.6 M_{\odot}$  region of the H-R diagram for all the tracks, clearly discrepant with the derived mass,  $\sim 1 M_{\odot}$ . It seems very unlikely that the distance to UZ Tau E could be  $\sim 60\%$  of the nominal 140 pc. Rather, the assumption that  $i_* = i_{\text{CO}}$  is probably wrong; the circumbinary disk and binary star orbits appear not to be coplanar. The spectroscopic binary orbit will be resolvable by the next generation space-borne astrometric missions so a precision measurement of the orbital parameters should be possible within a decade.

*GG Tau*.—White et al. (1999) compared the  $(L, T_{\text{eff}})$  positions of GG Tau Aa and Ab, the components of the  $\sim 0''.25$  separation binary at the center of the circumbinary ring we observed, with PMS evolutionary tracks calculated by Swenson et al. (1994), d'Antona & Mazzitelli (1994), DM97, and BCAH. They used the effective temperature scales for main-sequence dwarfs drawn from the works of Ryan, Norris, & Bessel (1991), Leggett (1996), and Luhman &

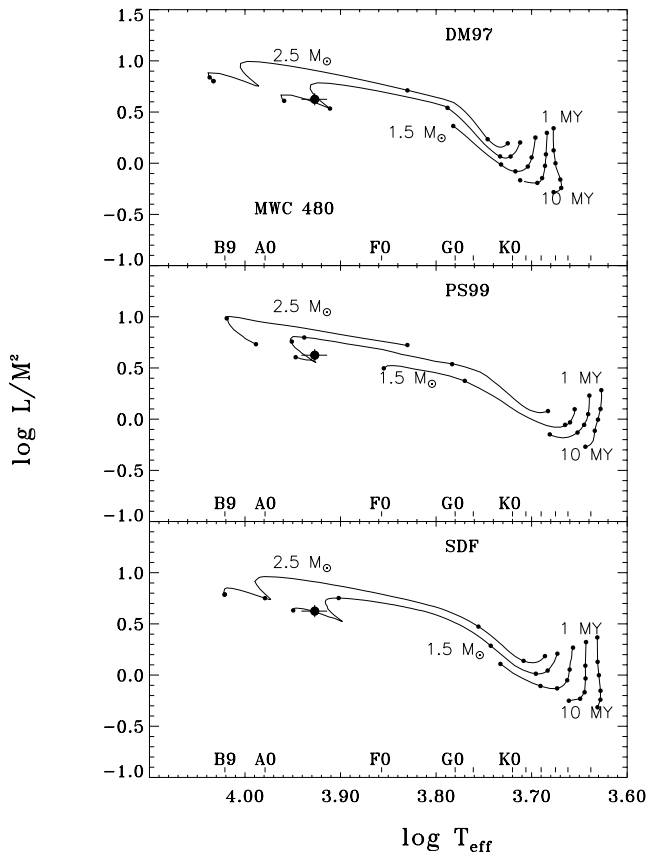


FIG. 4.—(Top)  $L/M^2$  vs.  $T_{\text{eff}}$  for the HAeBe star MWC 480 plotted with DM97 tracks for stars of mass 1.0, 1.2, 1.5, 2.0, and  $2.5 M_{\odot}$ . The dots indicate ages 1, 2, 3, 5, 7, and 10 MY. For the  $2.5 M_{\odot}$  track, the isochrone dots stop at 7 Myr—at this age the star is on the main sequence. (Middle) Same but for tracks calculated by PS99. The indicated ages are 1, 2, 3, 5, and 10 MY. The  $2.5 M_{\odot}$  star is on the main sequence at 5 Myr. (Bottom) Same but for SDF tracks. The range of masses and indicated ages are the same as for DM97.

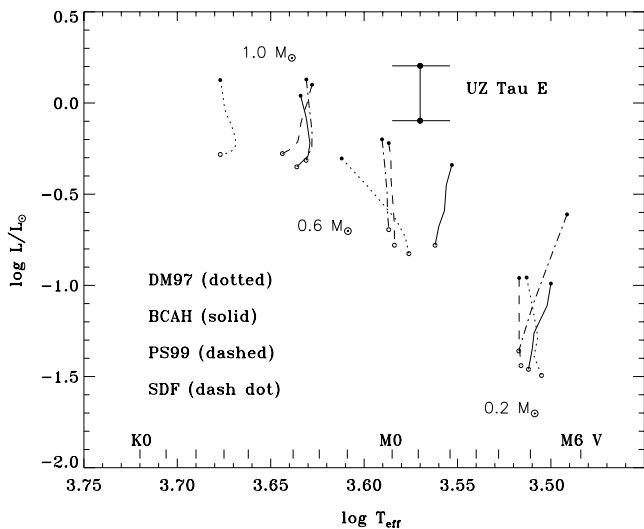


FIG. 5.—The primary of the spectroscopic binary UZ Tau E on an H-R diagram with evolutionary tracks plotted in the same format as in Fig. 3. The system spectral type M1 is assumed to apply to the primary with an uncertainty of  $\pm 1$  subclass. Its luminosity is plotted in the range from total system luminosity to half this value. If the inclinations of the circumbinary CO disk and the stellar binary are assumed to be the same, the mass of the primary is  $1.0 \pm 0.08 M_{\odot}$  (see text).

Rieke (1998). They found that the tracks calculated by BCAH were the most consistent with the total dynamical system we have measured and the expected coevality of the components. The BCAH indicated an age between 1 and 2 Myr.

Figure 6 shows a similar comparison with the tracks of DM97, BCAH, PS99, and SDF. The difference between the temperature scale used by White et al. (1999) and Kenyon & Hartmann’s (1995) temperature scale is unimportant at the effective temperatures of GG Tau Aa and Ab. The BCAH tracks suggest primary and secondary masses of  $\sim 0.8$  and  $\sim 0.7 M_{\odot}$ , and age 1–2 Myr, in agreement with White et al.’s finding. The PS99 and SDF tracks suggest similar masses and age. The DM97 tracks also indicate a young age for the components, in this case less than 1 Myr. The total mass indicated by DM97’s tracks,  $\sim 0.95 M_{\odot}$ , is significantly lower than our measured value. To reconcile it with the measured mass would require that the GG Tau system lie at distance  $\sim 103$  pc, which seems unlikely.

## 5. SUMMARY AND SUGGESTIONS FOR FUTURE WORK

Our results indicate that

1. Stellar masses can be measured dynamically by the rotation of their circumstellar disks with high enough precision, less than 5%, that meaningful tests of calculations of pre-main-sequence evolution are possible.

2. The BCAH, PS99, and SDF models in general are in reasonable agreement with the measured dynamical masses at the average distance to the Taurus SFR. To force agreement between the DM97 models and mass measurements for stars in the  $\sim 0.7$  to  $1 M_{\odot}$  range (LkCa 15, GM Aur, and the components of GG Tau) would require that these stars lie at distances 100–115 pc, which seem unacceptably near. This is a consequence of the apparently warmer photospheres of DM97’s models for stars close to  $1 M_{\odot}$ .

3. Consistency of the position of the HAeBe star MWC 480 with respect to DM97, PS99, and SDF’s tracks suggest it lies on the far side of the Taurus SFR at  $\sim 170$  pc.

Our tests of the pre-main-sequence tracks are limited by our present ignorance of actual distances to individual stars. We anticipate that this limitation will be overcome by precision distances that will be measured by the astrometric observatories currently under construction (e.g., FAME, GAIA, and SIM). All our measurements at present pertain to stars with  $M > 0.5 M_{\odot}$ , so we have been unable to test the models at the lowest end of the stellar mass spectrum. This is a serious limitation and results, at least in part, from the range of masses of stars formed in the Taurus SFR. We look forward to the capabilities of the ALMA millimeter-wave interferometric array that will open the rich Orion SFR to investigation. Conversion of the observationally derived parameter, spectral type, to that provided by the models,  $T_{\text{eff}}$ , is a lingering source of uncertainty, particularly at the lowest masses. Since stars contracting to the main sequence represent a range of surface gravities, the conversion may depend on the stars’ ages. Relief from this problem should become available soon as the model calculations that include stellar atmospheres provide diagnostics such as color indices and model spectra for closer comparison with the observations. We look forward to a fruitful decade ahead.

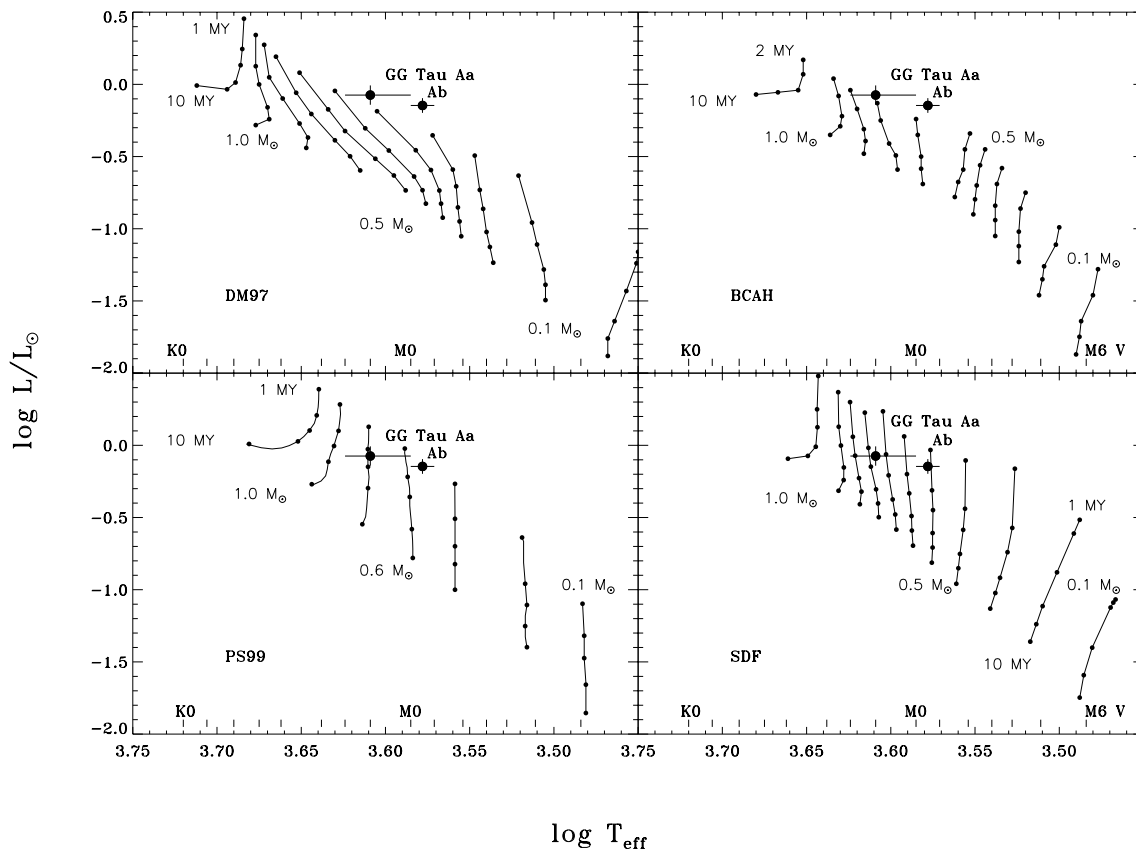


FIG. 6.—(Upper left-hand panel) Components of GG Tau, Aa and Ab, plotted on H-R diagrams showing the DM97 tracks. Masses and indicated ages are the same as in Fig. 3. (Upper right-hand panel) Same, but using BCAH tracks, presented in same format as corresponding panel in Fig. 3. (Lower left-hand panel) Same, but for PS99 tracks, in same format as corresponding panel Fig. 3. (Lower right-hand panel) Same, but for SDF tracks, following the format of Fig. 3.

We thank I. Baraffe, J. Bouvier, G. Chabrier, C. Dougados, M. Forestini, F. Palla, S. Stahler, and L. Siess for helpful conversations and communicating results before publication. This work began as a collaboration with G. Duvert and F. Ménard; we thank them for their advice and help in its early stages. We thank the referee for a prompt and helpful report. This paper was begun during M. S.'s sabbatical visit at the Observatoire de Grenoble; M. S. thanks G. Duvert and C. Perrier for making it possible and

for their hospitality. The work of M. S. was supported in part by NSF Grants 94-17191 and 98-19694.

*In memoriam:* The Plateau de Bure interferometer was affected by two transportation tragedies in 1999. These caused the death of 25 individuals, including six members of the IRAM staff and two from INSU-CNRS. We dedicate this work to the memory of the victims, especially our colleagues B. Aubeuf, F. Gillet, H. Gontard, D. Lazaro, R. Prayer, and P. Vibert.

#### REFERENCES

- Altenhoff, W. J., Strittmatter, P. A., & Wendker, H. J. 1981, *A&A*, 93, 48  
 Baraffe, I., et al. 1998, *A&A*, 337, 403 (BCAH)  
 Bertout, C., Arenon, F., & Robichon, N. 1999, *A&A*, 352, 574  
 Casey, B. W., et al. 1998, *AJ*, 115, 1617  
 d'Antona F., & Mazzitelli, I. 1997, *Mem. Soc. Astron. Italiana*, 68, 807 (DM97)  
 ———. 1994, *ApJS*, 90, 467  
 Dutrey, A., Guilloteau, S., & Simon, M. 1994, *A&A*, 286, 149 (DGS94)  
 Dutrey, A., et al. 1996, *A&A*, 309, 493  
 ———. 1998, *A&A*, 338, L63  
 Duvert, G., et al. 1998, *A&A*, 332, 867  
 ———. 2000, *A&A*, 355, 165  
 Favata, F., et al. 1998, *A&A*, 335, 218  
 Guilloteau, S., et al. 1992, *A&A*, 262, 624  
 Guilloteau, S., & Dutrey, A. 1998, *A&A*, 339, 467 (GD98)  
 Guilloteau, S., Dutrey, A., & Simon, M. 1999, *A&A*, 348, 570  
 Gullbring, E., Hartmann, L., Briceño, C., & Calvet, N. 1998, *ApJ*, 492, 323  
 Hartigan, P., Edwards, S., & Ghandour L. 1995, *ApJ*, 452, 736  
 Hartigan, P., Strom, K. M., & Strom, S. E. 1994, *ApJ*, 427, 961  
 Jensen, E. L. N., Koerner, D. W., & Mathieu, R. D. 1996, *AJ*, 111, 2431  
 Kenyon, S. J., Dobrzycka, D., & Hartmann, L. 1994, *AJ*, 108, 1872  
 Kenyon, S. J., & Hartmann, L. 1995, *ApJS*, 101, 117  
 Leggett, S. K., et al. 1996, *ApJS*, 104, 117  
 Luhman, K. L. 1999, *ApJ*, 525, 466  
 Luhman, K. L., & Rieke, G. H. 1998, *ApJ*, 497, 354  
 Malfait, K., et al. 1998, *A&A*, 331, 211  
 Mannings, V., & Sargent, A. I. 1997, *ApJ*, 490, 792  
 Mathieu, R. D., Martini, E. L., & Maguzzo, A. 1996, *BAAS*, 28, 920 (Abstract No. 60.05)  
 Palla, F., & Stahler, S. W. 1999, *ApJ*, 525, 772 (PS99)  
 Ryan, S. G., Norris, J. E., & Bessell, M. S. 1991, *AJ*, 102, 303  
 Siess, L., Dufour, E., & Forestini, M. 2000, *A&A*, 358, 593 (SDF)  
 Swenson, J. H., et al. 1994, *ApJ*, 425, 286  
 Thé, P. S., de Winter, D., & Pérez, M. R. 1994, *A&AS*, 104, 315  
 van den Ancker, M. E., de Winter, T., & Tjin A Djie, H. R. E. 1998, *A&A*, 330, 145  
 White, R. J., et al. 1999, *ApJ*, 520, 811